Electronic Supplementary Material (ESI) for RSC Advances.

Supporting information

Controlling the self-assembly and optical properties of gold nanoclusters and gold nanoparticles biomineralized with Bovine Serum Albumin

Birgitte H. McDonagh,[a] Gurvinder Singh,[b] Sulalit Bandyopadhyay,[a] Sina M. Lystvet,[a] Joseph A. Ryan,[c] Sondre Volden,[a] Eugene Kim,[d] Ioanna Sandvig,[e,f] Axel Sandvig,[f,g] Wilhelm R. Glomm[a, h]

[a.] *Ugelstad Laboratory, Department of Chemical Engineering, Norwegian University of Science and Technology (NTNU), 7491 Trondheim, Norway*
[b.] *Department of Materials Science and Engineering, Norwegian University of Science and Technology (NTNU), N-7491 Trondheim, Norway*
[c.] *Department of Chemistry, Iona College, New Rochelle, New York, USA*
[d.] *Department of Circulation and Medical Imaging, Norwegian University of Science and Technology (NTNU), N-7491 Trondheim, Norway*
[e.] *John Van Geest Centre for Brain Repair, Department of Clinical Neurosciences, University of Cambridge, CB2 OPY Cambridge, UK*
[f.] *Department of Neuroscience, Faculty of Medicine, Norwegian University of Science and Technology (NTNU), N-7491, Trondheim, Norway*
[g.] *Division of Pharmacology and Clinical Neurosciences, Department of Neurosurgery, Umeå University, 901 87 Umeå, Sweden*
[h.] *Sector for Biotechnology and Nanomedicine, SINTEF Materials and Chemistry, Trondheim, Norway*

*Correspondence to: birgitte.h.mcdonagh@ntnu.no

LSPR absorption of BSA-stabilized AuNPs and steady-state fluorescence emission of AuNCs

Figure S1 show the appearance of gold conduction band as observed with UV-Visible for both intrinsic and extrinsic synthesis. The spectrum shows the absorbance of gold nanoparticles at ~520nm for the extrinsic synthesis route.

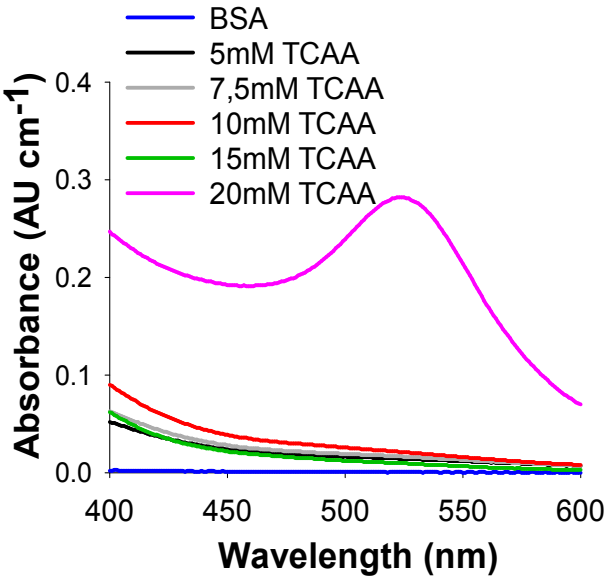

Figure S1: LSPR of BSA-stabilized AuNPS

Figure S2 show the Steady-state fluorescence spectra of fluorescent gold nanoclusters (λ_{ex} *=370 nm*) prepared via the extrinsic method. Figure S3 show the integral of the Trp emission (λ_{ex} *=295 nm)* as a function of TCAA.

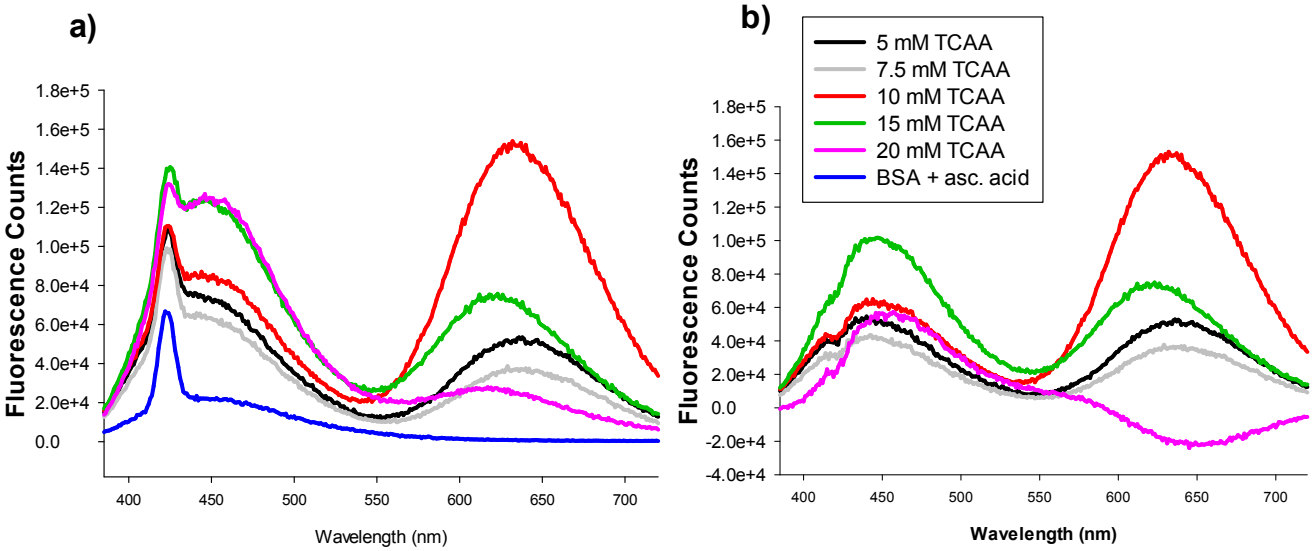

Figure S2. Spectra in a) show the emission of AuNCs with the contributing emission from BSA. Spectra b), the emission from BSA has been subtracted from all spectra, to show the contribution of only AuNCs.

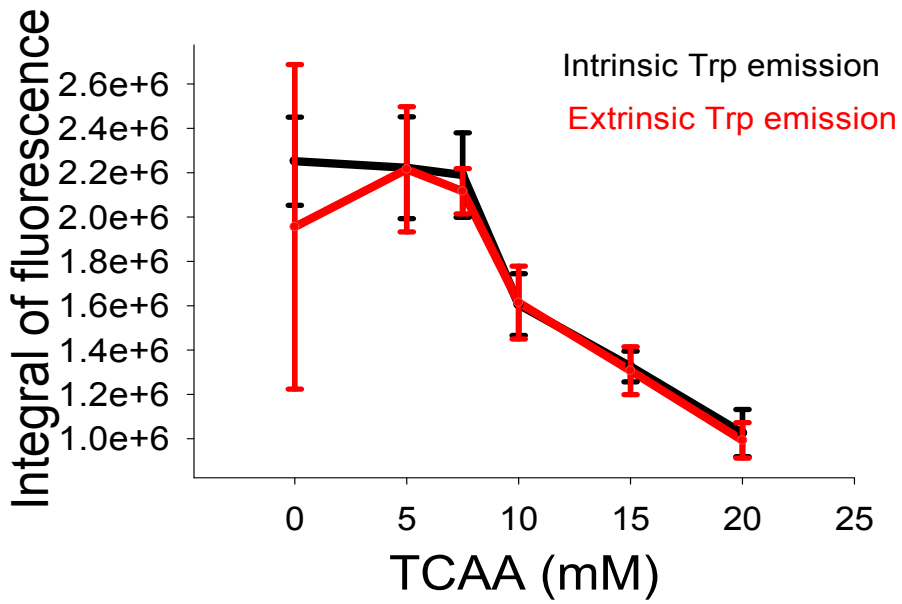

Figure S3: Integral of Trp emission (310-450 nm) as a function of TCAA. The red lines show the extrinsic Trp emission, while the black line show the intrinsic integral of Trp emission.

X-ray powder diffraction of BSA and BSA AuNPs

Figure S4 show the XRD-patterns for pure BSA (red line) and for BSA-AuNPs (black), and reveal crystalline structures of the BSA stabilized AuNPs.

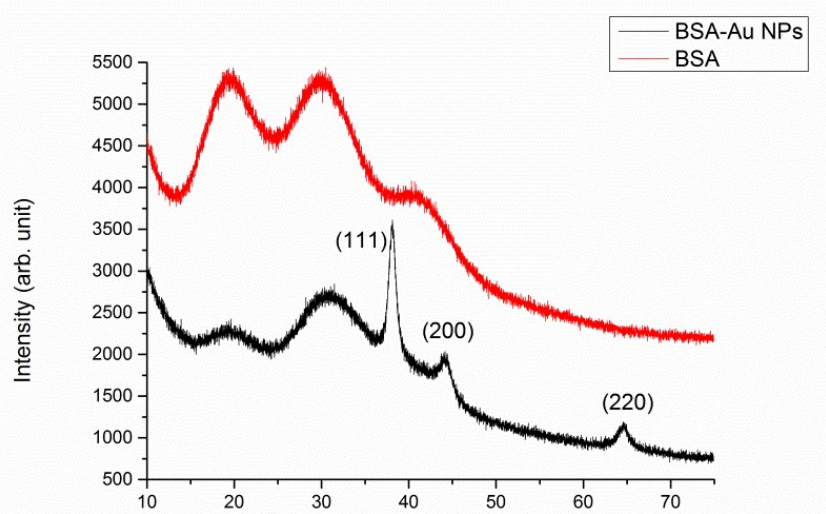

Figure S4: XRD patterns of BSA and BSA stabilized AuNPs

High-resolution inductive coupled plasma-mass spectrometry (ICP-MS)

Inductive- coupled plasma mass spectroscopy (ICP-MS) is a powerful technique for determining the elemental composition in a sample. The yield of gold determined by ICP-MS measurements is higher for the samples where nanoparticles are present, with a yield of 0.5%. The average yield for the intrinsic method is slightly higher than the extrinsic.

Table S1 show the amount of gold associated with samples with low amount of gold (7.5mM TCAA) and high amount of gold (20mM TCAA).

Table S1: Amount of gold associated with BSA determined by ICP-MS

Added TCAA (mM)	Gold intrinsic (ug/L)	Gold extrinsic (ug/L)	Average yield intrinsic (%)	Average yield extrinsic (%)
7.5	2.7 5.0 4.0	3.3 5.0 4.2	0.26±0.080	0.28±0.055
20	21.3 15.2 25.7	21.3 18.0 15.2	0.53±0.13	0.46±0.075

X-ray photoelectron spectroscopy (XPS)

Figure S5 show the X-ray photoelectron (XPS) spectra of two samples of BSA-gold.

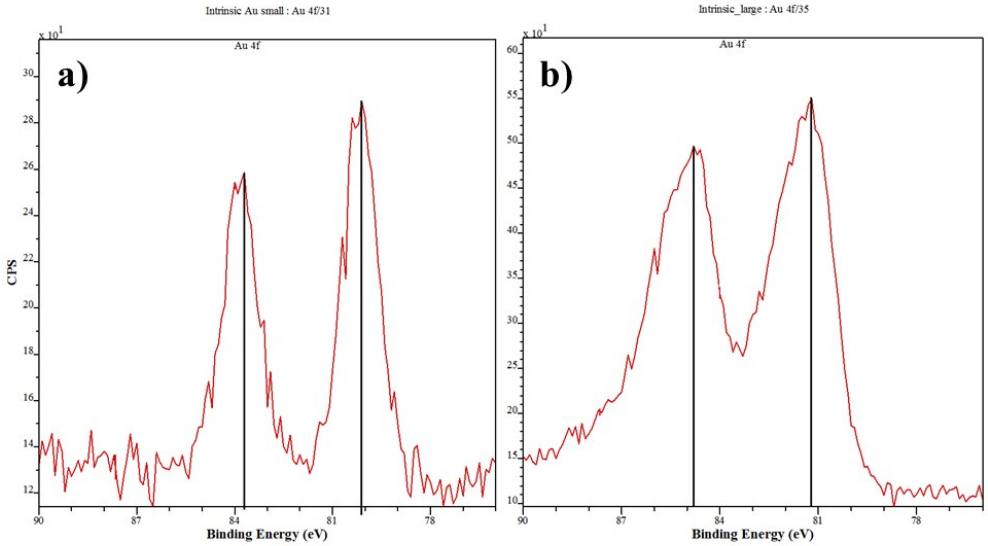

Figure S5: XPS spectra of **a)** BSA AuNCs and **b)** BSA AuNPs synthesized via the Intrinsic protocol. The AuNCs were synthesized with 5mM TCAA, while the AuNPs were synthesized with 20mM TCAA.

Time Correlated Single Photon Counting (TCSPC)

Time-correlated single-photon counting (TCSPC) measures the intensity decay of fluorophores on a nanosecond timescale.[7] Fluorescence lifetime measurements can give information about variation in the local environment of a fluorophore [8,9] and conformational changes in proteins. [10,11] TCSPC was performed with a 280 nm LED (λ_{ex}=*280nm*), and measuring the emission at 360 nm (λ_{em}=*360nm*). The fractional contribution of each decay time to the steady-state intensity, *f,* is determined from the decay times, *T,* and *B* which is the relative population of the components at *t* = 0, as shown in equation S1. [7]

$$f_i = \frac{B_i T_i}{\sum_j B_j T_j} \quad \text{(S1)}$$

All samples were best fit by biphasic decay, yielding one short (T_1) and one long (T_2) lifetime and their relative populations B_1 and B_2.

Table S2: Lifetimes and Populations

Synthesis	TCAA (mM)	T1 (ns)	B1 (%)	T2 (ns)	B2 (%)
Intrinsic	0	1.5±0.021	33.2±0.18	4.9±0.027	8.1±0.0049
	5	1.1±0.021	37.5±0.22	4.4±0.030	8.3±0.0048
	7,5	0.91±0.015	41.6±0.23	4.3±0.033	7.0±0.0043
	10	0.47±0.020	69.6±0.40	3.5±0.047	5.7±0.0041
	15	0.38±0.018	91.8±0.48	3.6±0.088	3.1±0.0029
	20	0.24±0.0083	160.4±0.85	3.7±0.095	1.8±0.0022
Extrinsic	0	2.04±0.031	22.7±0.13	5.9±0.028	8.68±0.0046
	5	1.63±0.027	26.5±0.14	4.7±0.033	6.9±0.0038
	7,5	1.45±0.027	27.6±0.15	5.4±0.033	7.03±0.038
	10	1.09±0.021	35.0±0.17	5.1±0.047	4.5±0.030
	15	0.81±0.017	40.9±0.20	5.5±0.052	3.6±0.023
	20	0.43±0.013	68.9±0.37	5.0±0.058	3.7±0.023

From 7.5mM-10mM TCAA, there is a large decrease in T1 and T2 for both the intrinsic and extrinsic synthesis. At 10mM TCAA, steady-state fluorescence data show an increased growth of large AuNCs, indicating that large AuNCs induce more prominent conformational changes compared to small AuNCs. From 7.5-10mM, the T1 for the intrinsic synthesis is reduced by a factor of 2.7, while the extrinsic T1 is reduced by a factor of 2. Since the protein is the sole reducing agent in the intrinsic synthesis, shorter lifetimes could indicate that there are larger changes in the polypeptide chain when ascorbic acid is not present.

The lifetime populations for the intrinsic and extrinsic samples show that as the size of gold increases, there is an increased short lifetime population (B1), and a concerted decreased long lifetime population (B2). The short and long populations show the relative percentage of fluorophores for the short and long lifetimes, respectively. At concentrations below 7.5mM TCAA chi-squared values ($\chi^2 \sim 1$) indicated a good fit, while above 7.5mM TCAA chi-squared values ($\chi^2 > 2$) were less ideal. Increasing the exponential fit for samples with concentrations above 7.5mM, would give a better fit, but

with more contribution from noise. [7] The data above 7.5mM TCAA can therefore not be used quantitatively, but qualitatively to indicate what happens to the protein when the concentration of TCAA is increased.

The prominent increase in B1 at 10mM could be an effect of the large conformational changes in BSA that takes place when large AuNCs appear. At 10mM TCAA, steady-state data of Trp emission reveal large changes in protein conformation, which would greatly affect TCSPC data as well. Because the lifetimes were measured with a 280 nm LED, it could be that as BSA changes conformation, tyrosine residues are exposed and contribute to the emission, thus increasing the overall lifetime populations. [7,12] Overall, the results reveal the same trend of lifetimes and populations for BSA with or without ascorbic acid. With increased size of BSA-gold, the short (T1) and long (T2) lifetimes decreased, while the short lifetime populations (B1) increased and the long lifetime populations (B2) decreased. There is a large difference in the short and long lifetimes of native BSA and BSA with AuNPs (20mM TCAA) indicating that the fluorophore on average spends less time in the excited state, which is probably caused by an increased exposure to water or energy transfer to BSA-gold, or a combination of the two. [13] Increased quenching of Trp emission with size of BSA-gold was also observed with steady-state fluorescence, showing that the protein gradually changes conformation as a result of the gold size.

Toxicity assay on glioblastoma-astrocytoma cells

Misfolded proteins are usually devoid of normal biological activity and can aggregate or interact with cells in an unwanted manner. [14,15] For example, in Alzheimer's disease, neurodegeneration is caused by amyloid plaques formed by misfolded β-amyloid protein aggregation.[16,17] As shown earlier, the tryptophan emission intensity was found to be inversely proportional to the size of gold, meaning that the folding of BSA is more affected with larger species of gold. If BSA-AuNCs or BSA-AuNPs either do or do not aggregate or interact with cell membranes, they could be used in different applications. Biocompatible constructs of BSA-stabilized gold can be used as drug delivery vehicles, while BSA-stabilized gold that aggregate and interact with cell membranes can be used as a drug in itself.

To this end, we tested the interaction of our BSA stabilized AuNCs and AuNPs with glioblastoma-astrocytoma cells *in vitro* and thus assessed their suitability as potential drug delivery vehicles in the therapy of glioblastoma multiforme. Glioblastoma multiforme is the most common primary brain tumor in adults. [18,19] It is very aggressive [20] and exhibit low response to conventional chemotherapeutic drugs.[21] Despite advances in therapy, [19] the estimated median survival of affected patients is one year.[20] To our knowledge, this is the first reported study on BSA-stabilized gold interaction performed on brain cancer cells. Previously, we have shown that the protein is important for the stability and size-tunability of the gold nanoconstructs. [13] Recently, we showed that synthesis of Transferrin-stabilized AuNCs had large surface affinities towards monolayers, and tended to localize on cell membranes *in vitro.* [22]

Human glioblastoma astrocytoma cells (U-87 MG, Sigma Aldrich) were cultured in Eagle's Minimal Essential Medium (EMEM) with 1.25% gentamicin (Sigma) and 10% fetal bovine serum (Autogen Bioclear, Wiltshire, UK). The cultures were supplemented with 2mM L-Glutamine, 1% non-essential amino acids (NEAA) (Sigma), and 1mM sodium pyruvate (NaP) (Sigma). Cells were labelled with BSA, BSA-AuNCs and BSA-AuNPs at concentrations of BSA/media volume of 1mg/mL, and incubated at 37°C for 24 hours. Unlabelled glioblastoma-astrocytoma cultures, at the same stage of confluence, were used as controls. After labeling, a LIVE/DEAD® cell viability assay (Invitrogen, Life Technologies) was performed on glioblastoma-strocytoma cultures. LIVE/DEAD® solution was prepared in 4.5mL PBS with 2.7µL calcein (InVitrogen), and 12µL ethidium homodimer (Invitrogen), was added to each well at 1:1 (v/v) and left to react for 30 minutes at 37°C. A LIVE/DEAD assay is a method for quickly assessing if there is a substantial cell death in one cell population compared to another. By taking images of the same magnification in the same area for all samples (*i.e* in the centre of the cell plate), it is possible to get information of the overall cell death. In Figure S6, dead cells were counted and the average amount of dead cells per image was calculated.

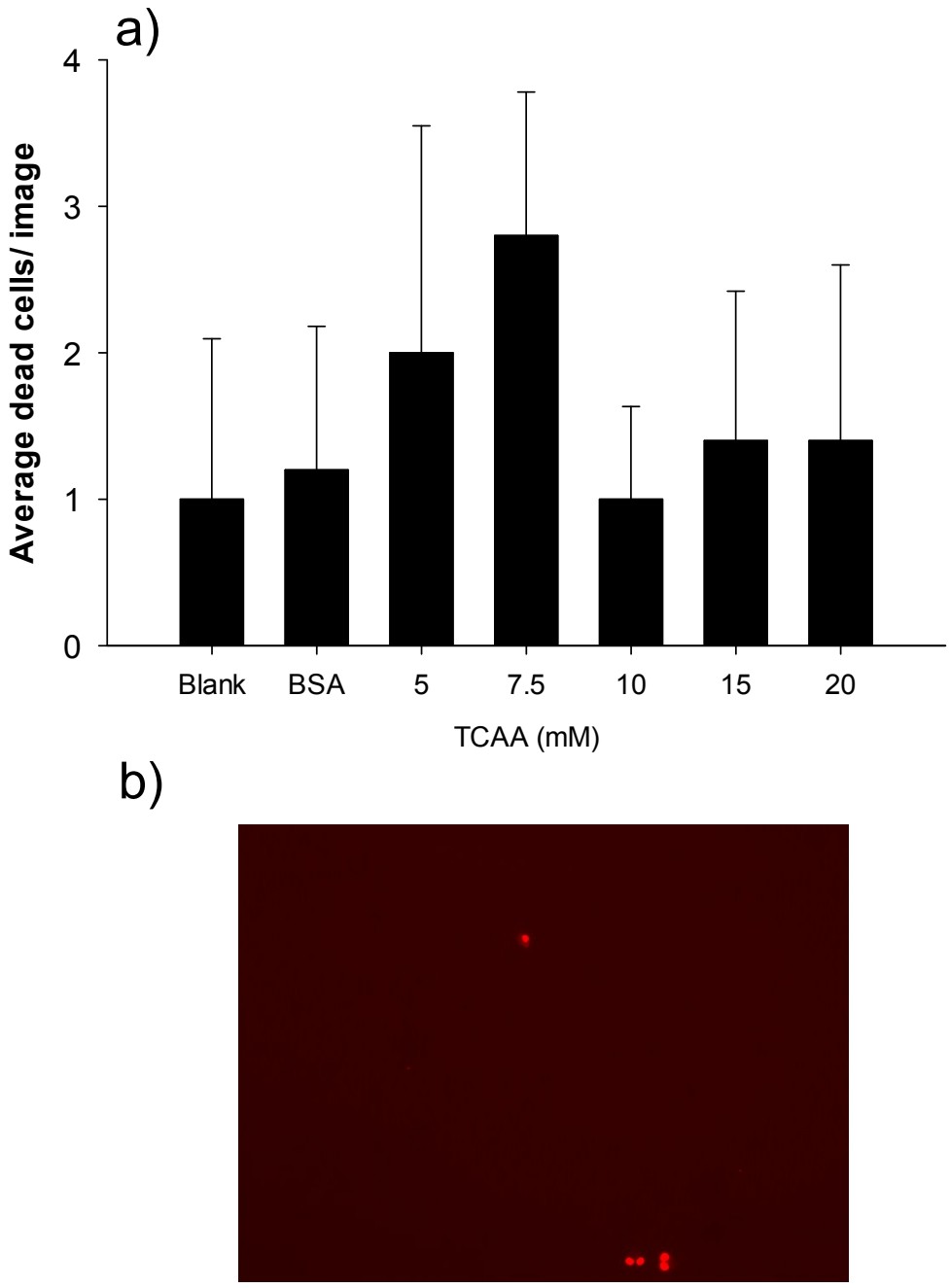

Figure S6: Dead glioblastoma-astrocytoma cells after incubation with BSA-AuNCs and BSA-AuNPs. a) Dead glioblastoma-astrocytoma cells counted with different concentrations of TCAA. The number of images counted per sample were 5. b) Glioblastoma astrocytoma cells grow very fast, and can therefore have multinucleate cells. In the example given, cell nuclei that lay very close to each other is counted as one cell.

No increased cell death was observed for any BSA-stabilized gold when compared to blank samples. This suggests that the BSA-stabilized gold described here do not aggregate or negatively impact cell membranes, which opens up for drug delivery applications. Compared to previous work on different proteins, these results indicate that the membrane affinity is also dependent on the protein. [13,22]

Computed Tomography

X-ray computerized tomography is a diagnostic imaging technique based on different tissue absorptions. For improved diagnostics, organic contrast agents (CAs) containing iodine is commonly used for enhanced attenuation. However, these CAs have very short circulation times. Because of their surface plasmon resonance, and inherently high attenuation coefficients (at 100keV gold has an attenuation coefficient of 5.16, while iodine has 1.94) AuNPs below 100nm have attracted a lot of attention as potential CT CAs. [48, 49] Here, three batches of large BSA-stabilized AuNPs were synthesized and their X-ray attenuation coefficients were measured (Figure S7). The size of the BSA-AuNPs determined the CT attenuation, with the smallest AuNPs giving the best attenuation. This is most likely caused by an increase in the surface area with decreasing size[50]. The mechanism of BSA-AuNP growth presented here can be used to determine the optimal size for CT imaging. The attenuation coefficient increase linearly with BSA-AuNP concentration which is comparable to what has been reported in previous studies with PEG-coated AuNPs for in vivo CT imaging. [51, 52]

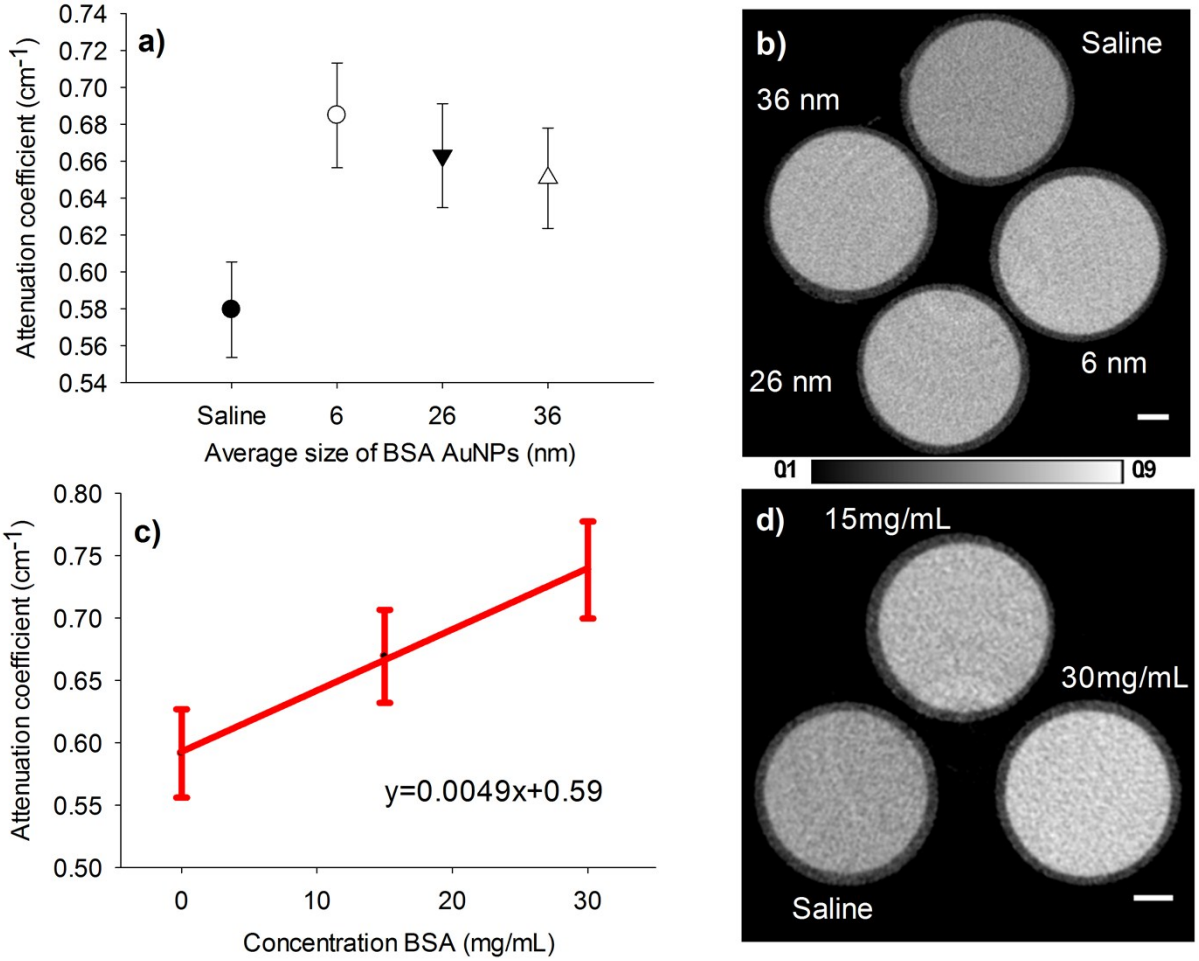

Figure S7: X-ray attenuation of BSA-AUNPs. a) With increasing size, the attenuation coefficient decrease. Saline is shown as a control. b) A slice of the reconstructed attenuation coefficient map of the CT phantom consisting of saline and three BSA-AuNP solutions (20 mg/ml) with different average sizes (6nm, 26nm, and 36nm). The scale bar is equal to 1 mm. c) Plot of the mean attenuation coefficient vs. BSA-AuNP concentration for the sample with the highest attenuation coefficient in a), *i.e* the sample containing average sized AuNPs of 6nm. Error bars indicate standard deviations. Solid line represents the linear regression line. d) Reconstructed image slice of the phantom from suspensions plotted in c).

For Computed tomography, sizes of the AuNPs were determined with ImageJ, and size fitting was determined with OriginPro 9.0 software. For the largest sample, a Gaussian fit was used, while for the two smallest samples a LogNormal fit was used. Figure S8 show some of the images acquired with STEM, and the calculated average and standard deviations.

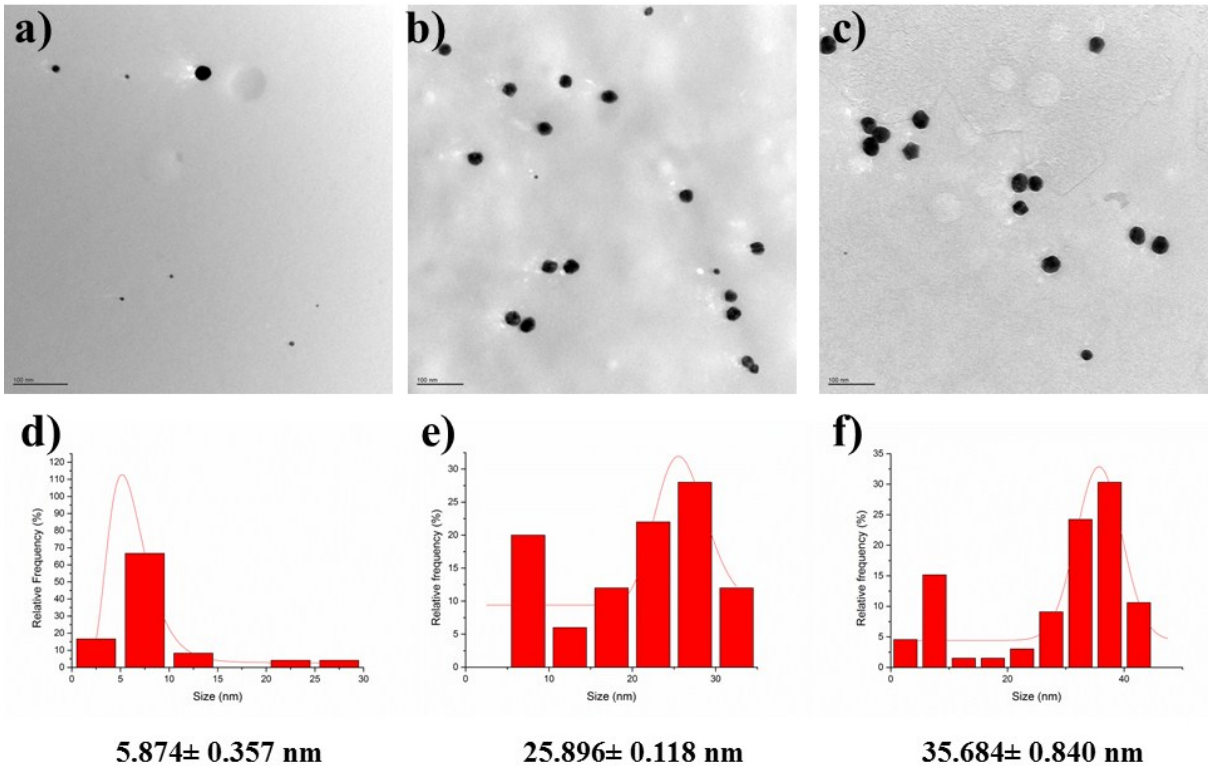

Figure S8: Size-determination of BSA AuNPs for Computed tomography. Images a)-c) show STEM-images of BSA-AuNPs. The error bar is 100 nm for all images. Graphs d)-f) show the fitted averages and standard deviations for the image a)-c), respectively.

Time-resolved steady-state fluorescence spectra of Trp (λ_{ex}=295nm) and AuNC emission (λ_{ex}=370nm)

Figure S9 displays steady-state fluorescence emission spectra (λ_{ex}=370nm) for six samples incubated with different amounts of TCAA and ascorbic acid (*i.e* the extrinsic method). Figure S10 show the tryptophan emission (λ_{ex}=295nm) from the same samples. Spectra were recorded over the time span of one week. The blue lines in each specter show the emission after 24 hours incubation time, while the red lines show the emission after 1 week (169 hours). The emission from Trp residues in BSA did not change much over the time course of 169 hours.

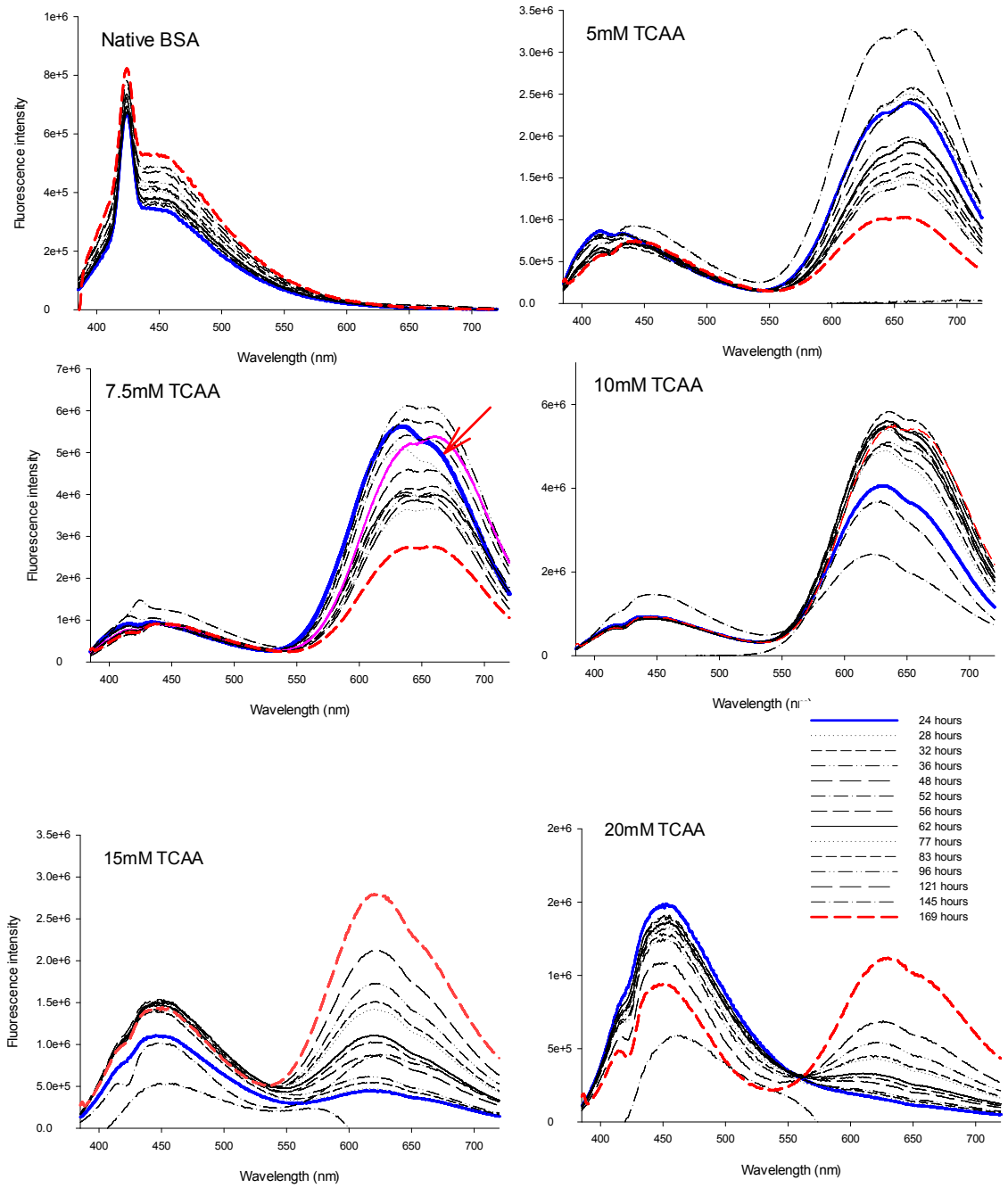

Figure S9: Time-dependent growth of gold nanoclusters followed by steady-state fluorescence, λ_{ex}=370nm. The six graphs show spectra of six different samples incubated with the extrinsic method taken over a time-period of one week. The BSA

spectra were subtracted for all samples to show only the contribution of the AuNC emission. The arrow indicates a shift in the shoulder from left to right after 62 hours.

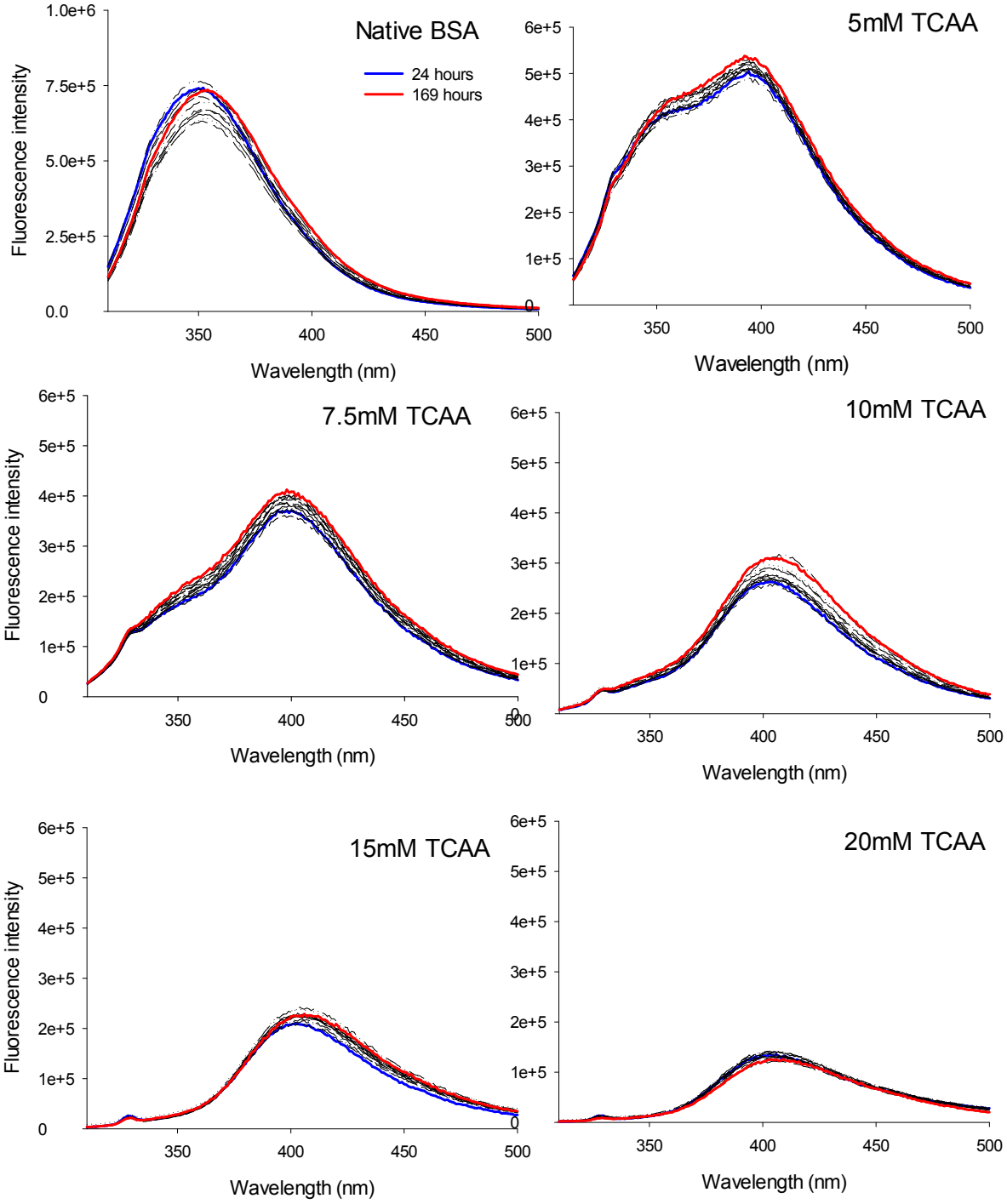

Figure S10: Changes in tryptophan emission with time and different gold precursor concentrations. Red line is after 24 hours, blue line is after one week. The purple line in graph *Native BSA* is the emission of tryptophan after 52 hours.

The integral of the Trp emission as a function of time is given in figure S11.

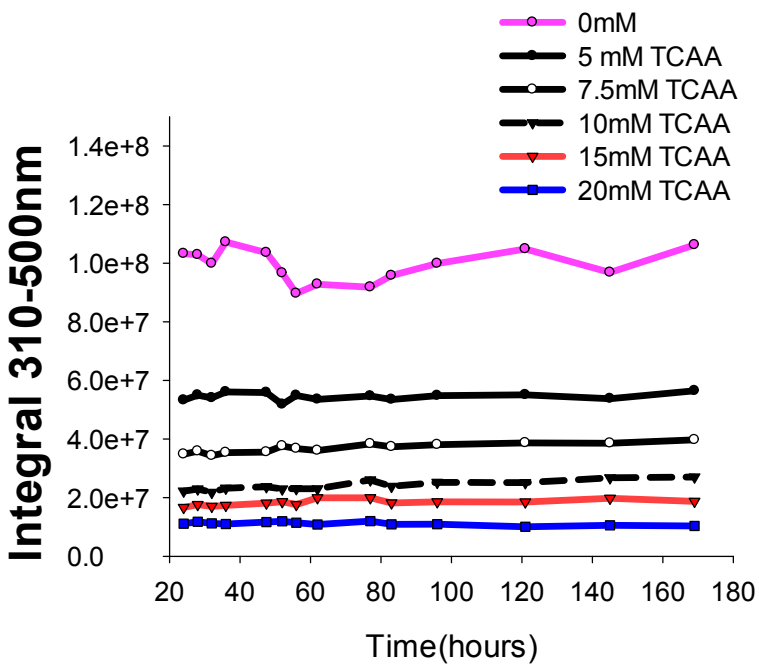

Figure S11: Trp emission integral as a function of time and concentration of TCAA.

References:

(1) Peters, S.; Peredkov, S.; Neeb, M.; Eberhardt, W.; Al-Hada, M. *Surf. Sci.* **2013**, *608*, 129.

(2) Le Guével, X.; Hötzer, B.; Jung, G.; Hollemeyer, K.; Trouillet, V.; Schneider, M. *J. Phys. Chem. C* **2011**, *115*, 10955.

(3) Tanaka, A.; Takeda, Y.; Imamura, M.; Sato, S. *Physical Review B* **2003**, *68*, 195415.

(4) McArthur, S. L. *Surf. Interface Anal.* **2006**, *38*, 1380.

(5) Sezen, H.; Suzer, S. *Thin Solid Films* **2013**, *534*, 1.

(6) Hajati, S.; Tougaard, S. *Anal. Bioanal. Chem.* **2010**, *396*, 2741.

(7) Lakowicz, J. R. *Principles of Fluorescence Spectroscopy*; 3 ed.; Springer: USA, 2006.

(8) Yuan, C. T.; Chou, W. C.; Tang, J.; Lin, C. A.; Chang, W. H.; Shen, J. L.; Chuu, D. S. *Opt. Express* **2009**, *17*, 16111.

(9) Castelli, F.; White, H. D.; Forster, L. S. *Biochemistry* **1988**, *27*, 3366.

(10) Julien, O.; Wang, G.; Jonckheer, A.; Engelborghs, Y.; Sykes, B. D. *Proteins: Structure, Function and Bioinformatics* **2012**, *80*, 239.

(11) Hochstrasser, R. M.; Negus, D. K. *Proc. Natl. Acad. Sci. U. S. A.* **1984**, *81*, 4399.

(12) Lystvet, S. M.; Volden, S.; Yasuda, M.; Halskau Jr, O.; Glomm, W. R. *Nanoscale* **2011**, *3*, 1788.

(13) Lystvet, S. M.; Volden, S.; Singh, G.; Yasuda, M.; Halskau, O.; Glomm, W. R. *RSC Advances* **2013**, *3*, 482.

(14) De Paoli Lacerda, S. H.; Park, J. J.; Meuse, C.; Pristinski, D.; Becker, M. L.; Karim, A.; Douglas, J. F. *ACS Nano* **2010**, *4*, 365.

(15) Chiti, F.; Dobson, C. M. 2006; Vol. 75, p 333.

(16) Polymeropoulos, M. H.; Lavedan, C.; Leroy, E.; Ide, S. E.; Dehejia, A.; Dutra, A.; Pike, B.; Root, H.; Rubenstein, J.; Boyer, R.; Stenroos, E. S.; Chandrasekharappa, S.; Athanassiadou, A.; Papapetropoulos, T.; Johnson, W. G.; Lazzarini, A. M.; Duvoisin, R. C.; Di Iorio, G.; Golbe, L. I.; Nussbaum, R. L. *Science* **1997**, *276*, 2045.

(17) Walsh, D. M.; Klyubin, I.; Fadeeva, J. V.; Cullen, W. K.; Anwyl, R.; Wolfe, M. S.; Rowan, M. J.; Selkoe, D. J. *Nature* **2002**, *416*, 535.

(18) Würth, R.; Barbieri, F.; Florio, T. *BioMed Research International* **2014**, *2014*.

(19) Yuan, X.; Curtin, J.; Xiong, Y.; Liu, G.; Waschsmann-Hogiu, S.; Farkas, D. L.; Black, K. L.; Yu, J. S. *Oncogene* **2004**, *23*, 9392.

(20) Suvà, M. L.; Riggi, N.; Janiszewska, M.; Radovanovic, I.; Provero, P.; Stehle, J. C.; Baumer, K.; Le Bitoux, M. A.; Marino, D.; Cironi, L.; Marquez, V. E.; Clément, V.; Stamenkovic, I. *Cancer Res.* **2009**, *69*, 9211.

(21) Pallini, R.; Ricci-Vitiani, L.; Banna, G. L.; Signore, M.; Lombardi, D.; Todaro, M.; Stassi, G.; Martini, M.; Maira, G.; Larocca, L. M.; De Maria, R. *Clin. Cancer. Res.* **2008**, *14*, 8205.

(22) McDonagh, B. H.; Volden, S.; Lystvet, S. M.; Singh, G.; Ese, M.-H.; Ryan, J. A.; Lindgren, M.; Sandvig, A.; Sandvig, I.; Glomm, W. R. *Nanoscale* **2015**.